Supporting information

Tailoring the Electrocatalytic Activity and Selectivity of Pt(111) through Cathodic Corrosion

Thomas J.P. Hersbach,[1†‡]* Chunmiao Ye,[1] Amanda C. Garcia[1§] and Marc T.M. Koper[1◊]*

[1]Leiden Institute of Chemistry, Leiden University, P.O. Box 9502, 2300 RA, Leiden, The Netherlands

[†]Present address: Stanford Synchrotron Radiation Lightsource, SLAC National Accelerator Laboratory, Menlo Park, California 94025, United States of America

[§]Present address: Faculty of Science, Van 't Hoff Institute for Molecular Sciences, University of Amsterdam, Science Park 904, 1098 XH, Amsterdam, The Netherlands

*Corresponding Authors

[‡]Email: hersbach@slac.stanford.edu

[◊]Email: m.koper@lic.leidenuniv.nl

Contents

Electrodes employed in this study

Figure S1 displays normalized blank cyclic voltammograms (CVs) of the electrodes used in the current study. The shape of these voltammograms is in good agreement with literature voltammograms of corresponding single- and polycrystalline Pt electrodes.[1,2] The voltammograms were normalized using the integrated hydrogen desorption current densities, without correcting for the double layer.[1,2]

All ORR current densities in this article are reported by normalizing with respect to the *geometric* electrode surface area, as is appropriate when considering reactant mass transport through diffusion or convection.[3] The geometric surface areas of most of the employed electrodes differed by no more than 2% from the electrochemically calculated surface area. The only exception to this statement is Pt(111), for which the electrochemical surface area was 13% smaller than the geometric surface area. Similar deviations were obtained for a different Pt(111) crystal. For Pt(111), normalizing currents by the geometric surface area was therefore critical in calculating limiting current densities that match the Levich equation.
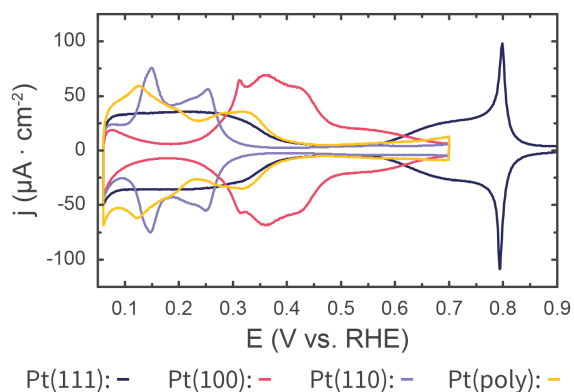

Pt(111): ━   Pt(100): ━   Pt(110): ━   Pt(poly): ━

Figure S1: Cyclic voltammograms of the employed electrodes: Pt(111), Pt(100), Pt(110) and Pt(poly). Voltammograms were recorded in 0.1 M HClO$_4$, at a scan rate of 50 mV·s^{-1}.

Blank voltammograms of large Pt(111) electrode

Figure S2 displays blank cyclic voltammograms of the 10-mm-diameter Pt(111) that was used for glycerol oxidation HPLC sample collection. The electrode was corroded for 1 minute at -3 V *vs.* RHE, in 10 M NaOH. As mentioned in the main text, this corrosion potential was not IR-corrected, so that the 'real' electrode potential during corrosion was approximately -2 V *vs.* RHE.

As can be seen in Figure S2, the uncorroded electrode displays the characteristic features of a Pt(111) single crystal, thus matching the smaller single crystal that was used in the other experiments in this work. After corrosion, the Pt(111) electrode exhibits signatures corresponding to (110) steps, (100) steps, and (100) terraces, as is also discussed in the main text. Though slightly more (110) sites are present than after IR-corrected corrosion of a smaller electrode at -3 V *vs.* RHE (Figure 4), the (100) features are well-developed in Figure S2.
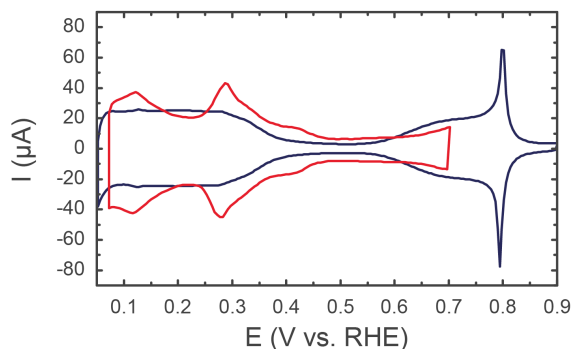
Before polarization: ─   After polarization: ─

Figure S2: Cyclic voltammograms of Pt(111) before (blue trace) and after (red trace) cathodic polarization in 10 M NaOH at -3 V vs. *RHE. Voltammograms were recorded in 0.1 M HClO4, at a scan rate of 50 mV·s^{-1}.*

Comparison of Pt(111) electrodes after cathodic corrosion in 1 M NaOH

Figure S3 shows CVs of Pt(111) after cathodic corrosion at various potentials in 1 M NaOH. The current traces in Figure S3 overlap well, which indicates that there are no significant differences in the post-corrosion voltammograms, as function of the corrosion potential.
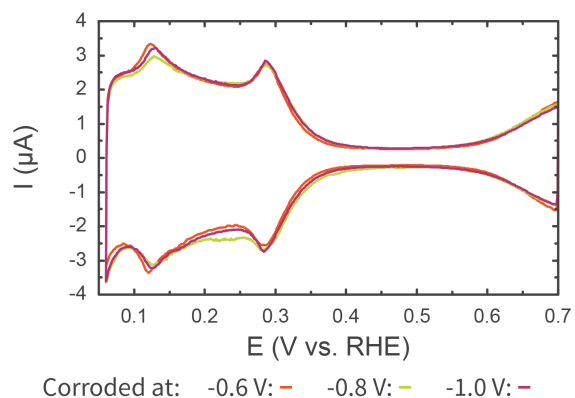

Corroded at: -0.6 V: —   -0.8 V: —   -1.0 V: —

Figure S3: Cyclic voltammograms of Pt(111) after cathodic corrosion at various potentials in 1 M NaOH. Voltammograms were recorded in 0.1 M HClO$_4$, at a scan rate of 50 mV·s^{-1}.

Validation of the HMRD setup

When using the hanging meniscus rotating disk (HMRD) configuration, one should verify that the working electrode behaves like a rotating disk electrode (RDE).[4] Specifically, the height of the electrode has to be controlled carefully:[4] if the electrode is too low, wetting of the side will occur and the catalytic activity of sites other than the desired facet will be probed. This causes an increased absolute slope in the Levich plot. In contrast, if the electrode is too high, the meniscus will be constrained. This leads to reduced mass transport and an offset in the ORR Levich plots.

Levich plots were therefore constructed for each electrode to verify the validity of the HMRD setup for the investigated system. A set of ORR voltammograms used for these Levich plots is displayed for Pt(111) Figure S4. The CVs contain no pronounced oscillations, which indicates proper concentric alignment of the single crystal. Furthermore, the voltammograms at 0, 200, 400 and 900 rpm contain the characteristic 'butterfly' feature around 0.8 V *vs.* RHE. The presence of the butterfly and the decrease of its intensity with increasing rotation rate is a strong sign of electrolyte cleanliness.[5,6]
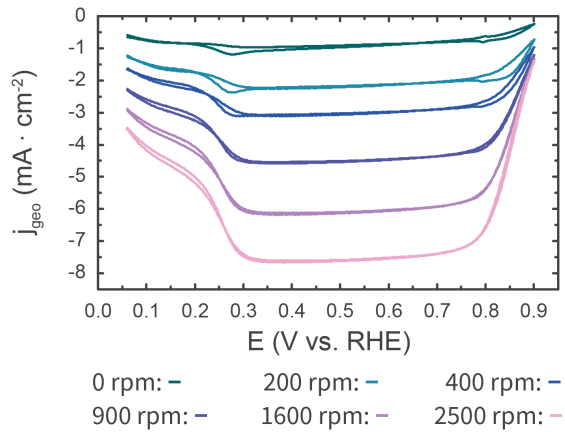

Figure S4: Cyclic voltammograms for oxygen reduction on Pt(111), at various rotation rates. Voltammograms were recorded in oxygen-saturated 0.1 M HClO₄, at a scan rate of 50 mV·s⁻¹.

Additional signs of the proper functioning of the HMRD setup can be seen in Figure S5, which shows exemplary Levich plots for each of the electrodes in this study. The theoretical Levich plots were calculated using the Levich equation:[7]

$$J_L = 0.62 \cdot n \cdot F \cdot D_{O_2}^{\frac{2}{3}} \cdot \omega^{\frac{1}{2}} \cdot \nu^{-\frac{1}{6}} \cdot C_{O_2}^* \tag{S1}$$

Here, n equals the amount of transferred electrons; F equals Faraday's constant; D_{O_2} equals the oxygen diffusion constant; ω equals the radial electrode rotation rate; ν equals the kinematic viscosity of the solution; and $C_{O_2}^*$ equals the oxygen concentration. For the studied system, the parameters take the following values: $n = 4$ for the conversion from O_2 to H_2O; $D_{O_2} = 1.67 \cdot 10^{-5}\ cm^2 s^{-1}$;[8] $\nu = 8.93 \cdot 10^{-3} cm^2 s^{-1}$;[9] and $C_{O_2}^* = 1.384\ mM$.[8]
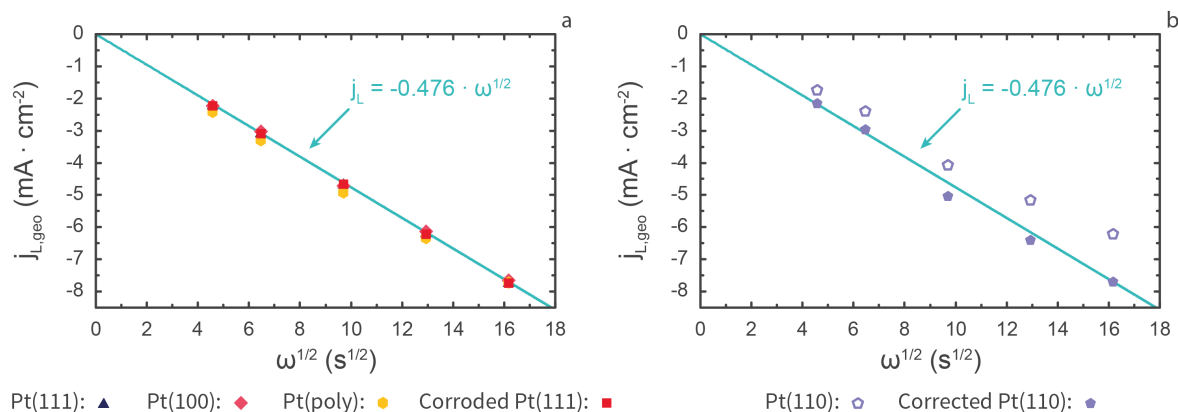
Figure S5: Levich plots for the ORR on Pt(111), Pt(100), Pt(poly) and Pt(111) which was corroded at -1.0 V vs. RHE in 1 M NaOH (a). Corrected and uncorrected Levich plots for the ORR on Pt(110) (b). Voltammograms for acquiring the plotted datapoints were recorded in 0.1 M HClO₄, at a scan rate of 50 mV·s⁻¹.

As can be seen in Figure S5a, the Pt(111), Pt(100), Pt(poly) and corroded Pt(111) electrodes are described well by the theoretical Levich plot: they exhibit zero or near-zero offsets and slopes within several percent of the theoretically expected value. However, Figure S5b demonstrates that the theoretical behavior is matched less well by Pt(110), for which 20% *lower* Levich slope is obtained. This change in slope is not due to wetting of the side of the electrode, which should increase the magnitude of the slope.[4] The slope change is also not related to dynamic changing of the meniscus shape during rotation, which should cause a vertical offset in the Levich plot.[4]

Instead, the slope change must be ascribed to a decrease in the apparent electrode area. This is demonstrated by 'correcting' the current densities by dividing them by the relative difference between the obtained current density and the theoretical current density at 2500 rpm. This corrected curve is represented by the filled pentagons in Figure S5b and matches the theoretical Levich plot well. The deviations from ideal diffusion behavior are therefore compensated for when normalizing the data as done in Figure 3 in the main text. After such normalization, the Pt(110) activity matches that of previously reported electrodes.[6,10] As such, the benchmarking results in Figure 3b in the main text confirm the validity of the employed setup.

Kinetic ORR current densities

The ORR activity of the electrodes can also be assessed by calculating kinetic current densities at 0.9 V *vs.* RHE. These kinetic current densities are calculated by rewriting the Levich equation to:[11]

$$\frac{1}{j} = \frac{1}{j_k} + B \cdot \omega^{-\frac{1}{2}}$$ (S2)

Here, j_k is the kinetic current density and B depends on the various parameters in the Levich equation. j_k is obtained from Equation S2 by plotting the inverse current density *versus* $\omega^{-\frac{1}{2}}$ in a Koutecky-Levich plot. From such a plot, the intercept is obtained through a linear least-squares fit and j_k is then obtained as the inverse of the intercept. The result of this procedure is plotted for all studied electrodes in Figure S6.
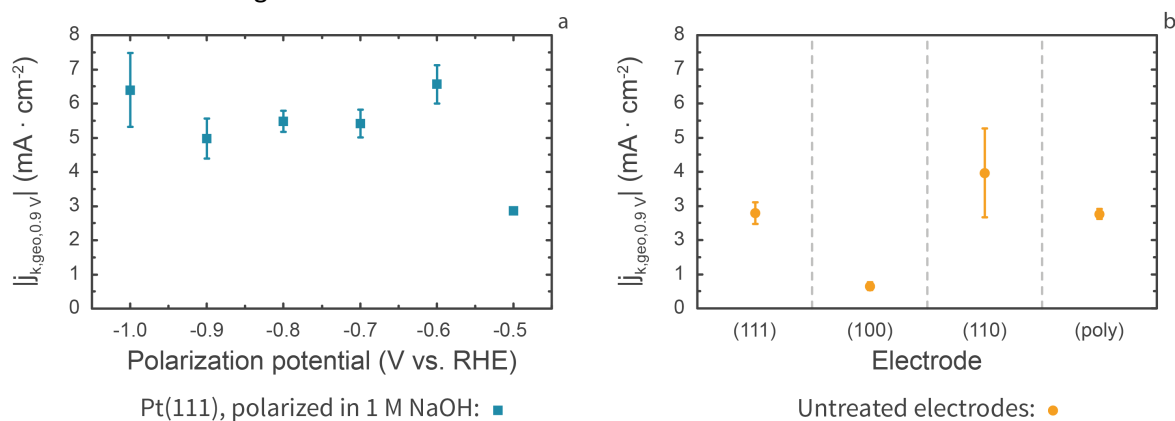

Figure S6: Kinetic ORR current densities of corroded Pt(111) (blue squares), as function of the polarization potential (a) and of uncorroded electrodes (yellow circles) (b). Rotation rate: 1600 rpm. Each data point is the average of 3 or more experiments. Error bars represent one standard deviation.

As can be seen, Figure S6 is in good qualitative agreement with Figure 3. The slightly larger error bars in Figure S6 are related to slight variations in the recorded current densities due to small variations in the meniscus height. Finally, it should be noted that the kinetic current density for Pt(110) in Figure S6 is *not corrected* for the aforementioned reduced surface area and is therefore underestimated.

Glycerol oxidation after corrosion in 5 M LiOH

This section will briefly elaborate on the effect of cathodically created step sites in cathodic corrosion. To do so, Figure S7a presents the cyclic voltammograms of a Pt(111) electrode before and after cathodic corrosion at -3.0 V *vs.* RHE, in 5 M LiOH. As can be seen in the Figure and in previous work,[12] corrosion in 5 M LiOH induces markedly less dramatic corrosion than in 10 M NaOH: only some (110) and (100) steps are created, as well as a minor amount of (100) terraces that is visible as an anodic shoulder of the (100) peak in the cyclic voltammogram after corrosion. Indeed, the overall amount of corrosion at -3.0 V *vs.* RHE in 5 M LiOH qualitatively resembles the amount of corrosion at -0.6 V *vs.* RHE in 1 M NaOH (Figure 1b).

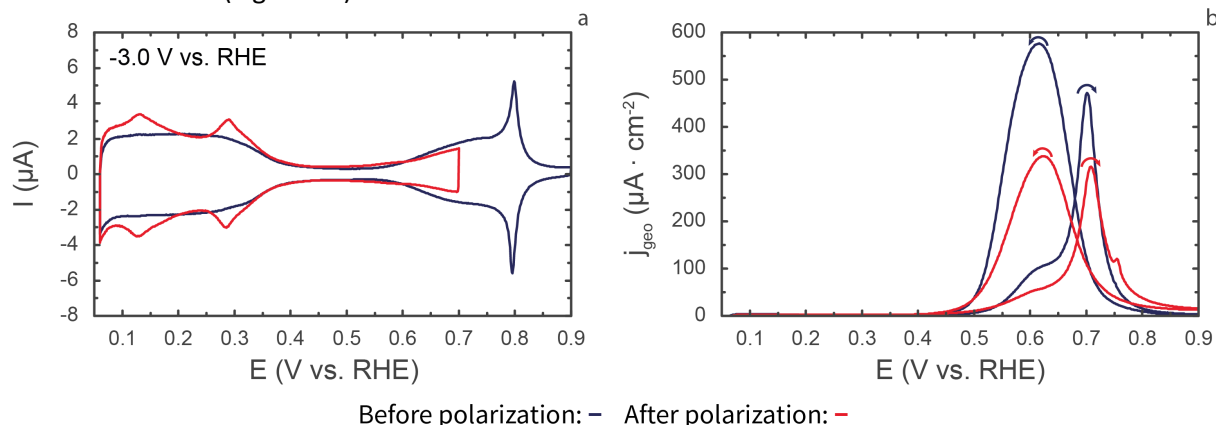Before polarization: −   After polarization: −

Figure S7: Blank cyclic voltammograms of Pt(111) before (blue trace) and after (red trace) cathodic polarization in 5 M LiOH at -3.0 V vs. *RHE (a) and glycerol oxidation voltammograms of the same electrodes (b). Blank voltammograms were recorded in 0.1 M HClO$_4$, at a scan rate of 50 mV·s^{-1}. Glycerol oxidation voltammograms were recorded in 0.5 M HClO$_4$ with 0.1 M glycerol, at 10 mV·s^{-1}.*

These created features have a much smaller effect on glycerol oxidation than those presented in the main text, as is apparent in Figure S7b. This Figure displays only a small peak at 0.75 V *vs.* RHE, which is associated with (100) terraces. The presence of this peak can be explained by the minor amount of (100) terraces that is identified in Figure S7a. It therefore appears that the additional (100) and (110) step sites have no noticeable effect on glycerol oxidation catalysis.

As in the section on page S-10, the described changes were found in an un-replicated exploratory experiment. However, consistent results were found for treatment at less cathodic potentials in both 5 M LiOH and 5 M NaOH. The results in Figure S7 are therefore a reliable illustration of the effect of cathodically created step sites on glycerol oxidation on Pt(111) in 0.5 M HClO$_4$.

ORR after corrosion in 10 M NaOH

If cathodic corrosion indeed optimizes the ORR through creating optimally sized concave sites on the electrode surface, there should be an optimal amount of cathodic corrosion. Before this optimum is reached, the creation of more 'optimized' sites will enhance catalysis. In contrast, corrosion beyond the optimum will create overlapping areas of cathodic corrosion and formation of sites that are bigger than ideally required. Beyond the optimum, the addition of catalytic sites should therefore cause a decrease in catalytic activity due to an impaired per-site activity. This effect is demonstrated here, through experiments of Pt(111), corroded in 10 M NaOH.

Voltammograms of Pt(111) after corrosion at and slightly below the onset potential in 10 M NaOH are displayed in Figure S8. This series of experiments was explorative in nature and was therefore performed once, with a different Pt(111) electrode than that was used in the main text.
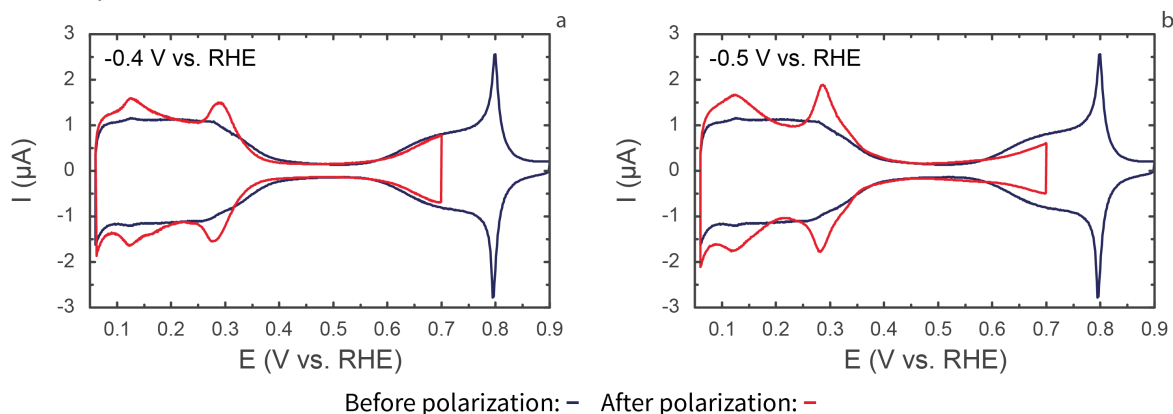

Before polarization: – After polarization: –

Figure S8: Cyclic Voltammograms of Pt(111) before (blue trace) and after (red trace) cathodic polarization in 10 M NaOH at -0.4 V vs. RHE (a) and -0.5 V vs. RHE (b). Voltammograms were recorded in 0.1 M HClO₄, at a scan rate of 50 mV·s⁻¹.

The electrode in Figure S8a appears similar to those in Figure 1 and Figure S3, with an approximately 15% apparent area increase. Indeed, the normalized ORR activity of this electrode at 0.9 V *vs.* RHE and 1600 rpm is similar to those in the main text: 0.32. In contrast, Figure S8b indicates significantly more (110) and (100) step sites after corrosion at -0.5 V *vs.* RHE and a roughly 25% area increase. The (100) peak also exhibits a small anodic shoulder, indicating the formation of a small amount of larger (100) terraces. Interestingly, the electrode has a *lower* normalized ORR activity of 0.27. In fact, the normalized ORR activity in these explorative experiments decreased monotonically with more negative corrosion potentials. The lowest normalized activity of 0.2 was reached at the most negative explored potential of -0.8 V *vs.* RHE. This trend confirms that corrosion beyond a certain point causes a decrease in ORR activity, even though blank cyclic voltammograms will indicate that more step sites are introduced overall. As such, the trend falls in line with the hypothesis that optimal ORR catalysis occurs on relatively small sites that present catalytic centers with an increased generalized coordination number.[13]

References

(1)   Gomez, R.; Orts, J. M.; Alvarez-Ruiz, B.; Feliu, J. M. Effect of Temperature on Hydrogen Adsorption on Pt(111), Pt(110), and Pt(100) Electrodes in 0.1 M HClO4. *J. Phys. Chem. B* **2004**, *108* (111), 228–238.

(2)   Chen, Q.-S.; Solla-Gullón, J.; Sun, S.-G.; Feliu, J. M. The Potential of Zero Total Charge of Pt Nanoparticles and Polycrystalline Electrodes with Different Surface Structure: The Role of Anion Adsorption in Fundamental Electrocatalysis. *Electrochim. Acta* **2010**, *55* (27), 7982–7994.

(3)   Bard, A. J.; Faulkner, L. R. Microscopic and Geometric Areas. In *Electrochemical Methods: Fundamentals and Applications*; Wiley: New York, 2001.

(4)   Villullas, H. M.; Teijelo, M. L. The Hanging-Meniscus Rotating Disk (HMRD) Part 1. Dependence of Hydrodynamic Behavior on Experimental Variables. *J. Electroanal. Chem.* **1995**, *384* (1–2), 25–30.

(5)   Gómez-Marín, A. M.; Rizo, R.; Feliu, J. M. Some Reflections on the Understanding of the Oxygen Reduction Reaction at Pt(111). *Beilstein J. Nanotechnol.* **2013**, *4* (1), 956–967.

(6)   Gómez-Marín, A. M.; Rizo, R.; Feliu, J. M. Oxygen Reduction Reaction at Pt Single Crystals: A Critical Overview. *Catal. Sci. Technol.* **2014**, *4* (6), 1685.

(7)   Bard, A. J.; Faulkner, L. R. Rotating Disk Electrode. In *Electrochemical Methods: Fundamentals and Applications*; Wiley: New York, 2001.

(8)   Wakabayashi, N.; Takeichi, M.; Itagaki, M.; Uchida, H.; Watanabe, M. Temperature-Dependence of Oxygen Reduction Activity at a Platinum Electrode in an Acidic Electrolyte Solution Investigated with a Channel Flow Double Electrode. *J. Electroanal. Chem.* **2005**, *574* (2), 339–346.

(9)   Wang, W.; Zheng, D.; Du, C.; Zou, Z.; Zhang, X.; Xia, B.; Yang, H.; Akins, D. L. Carbon-Supported Pd-Co Bimetallic Nanoparticles as Electrocatalysts for the Oxygen Reduction Reaction. *J. Power Sources* **2007**, *167* (2), 243–249.

(10)   Attard, G. A.; Brew, A. Cyclic Voltammetry and Oxygen Reduction Activity of the Pt{110}-(1×1) Surface. *J. Electroanal. Chem.* **2015**, *747*, 123–129.

(11)   Schmickler, W.; Santos, E. Convection Techniques. In *Interfacial Electrochemistry*; Springer Berlin: Heidelberg, 2010.

(12)   Hersbach, T. J. P.; McCrum, I. T.; Anastasiadou, D.; Wever, R.; Calle-Vallejo, F.; Koper, M. T. M. Alkali Metal Cation Effects in Structuring Pt, Rh, and Au Surfaces through Cathodic Corrosion. *ACS Appl. Mater. Interfaces* **2018**, *10* (45), 39363–39379.

(13)   Calle-Vallejo, F.; Tymoczko, J.; Colic, V.; Vu, Q. H.; Pohl, M. D.; Morgenstern, K.; Loffreda, D.; Sautet, P.; Schuhmann, W.; Bandarenka, A. S. Finding Optimal Surface Sites on Heterogeneous Catalysts by Counting Nearest Neighbors. *Science* **2015**, *350* (6257), 185–189.